摘要

化疗药物喜树碱 CPT 和基因药物 siPlk1 联合给药可以抑制癌症。为了保证两种药物能够同时被递送至病患部位，且 siPlk1 可以首先释放下调 Plk1 蛋白的表达而促进肿瘤细胞对喜树碱 CPT 的敏感性，课题构建了双重敏感-程序可控释放的喜树碱 CPT 前药阳离子脂质体/siPlk1 联合给药体系。通过 pH 和酯酶敏感的酯键将喜树碱和两性离子聚合物 PCB 连接以增加 CPT 的稳定性和载药率。将 CPT-PCB 前药与阳离子脂质 DDAB 结合制备基于 CPT 的阳离子脂质体，从而复合 siPlk1 构建联合给药体系。双重敏感的 CPT-PCB/siPlk1 联合给药体系能够将两种药物同时递送至肿瘤细胞，并且实现程序可控释放：即 siPlk1 利用 PCB 在内涵体中的质子化能力在孵育 4 h 时释放下调 Plk1 蛋白表达，而 CPT 在孵育 12 h 后持续释放。因此，该联合给药输递体系在体外能够发挥协同作用有效诱导肿瘤细胞凋亡。在体内实验中，能够将两种药物同时递送至肿瘤部位，协同抑制肿瘤生长，从而有效提高 CPT 和 siPlk1 在肿瘤治疗中的应用。

Biomaterials 35 (2014) 9731–9745

Contents lists available at ScienceDirect

Biomaterials

journal homepage: www.elsevier.com/locate/biomaterials

Dual sensitive and temporally controlled camptothecin prodrug liposomes codelivery of siRNA for high efficiency tumor therapy

Yan Li [a, b], Ruiyuan Liu [a, c], Jun Yang [a], Guanghui Ma [a], Zhenzhong Zhang [c, **], Xin Zhang [a, *]

[a] National Key Laboratory of Biochemical Engineering, Institute of Process Engineering, Chinese Academy of Sciences, Beijing 100190, PR China
[b] University of Chinese Academy of Sciences, Beijing 100049, PR China
[c] School of Pharmaceutical Sciences, Zhengzhou University, 100 Kexue Avenue, Zhengzhou 450001, PR China

ARTICLE INFO

Article history:
Received 13 June 2014
Accepted 12 August 2014
Available online 2 September 2014

Keywords:
Dual sensitive
Camptothecin prodrug
Poly(carboxybetaine)
Temporally controlled release
Combination therapy

ABSTRACT

The combination of chemotherapeutic drug camptothecin (CPT) and siPlk1 could prohibit cancer development with combined effects. To ensure the two drugs could be simultaneously delivered to tumor region with high loading content, and the modulator siPlk1 could be released in advance to down-regulate the Plk1 expression to improve the sensitivity of CPT to cancer cells, dual sensitive and temporally controlled CPT prodrug based cationic liposomes with siPlk1 codelivery system was constructed. The pH-sensitive zwitterionic polymer poly(carboxybetaine) (PCB) was conjugated with CPT through pH and esterase-sensitive ester bond to enhance the stability and loading content of CPT. CPT-based cationic liposomes consisted of CPT-PCB prodrug and cationic lipid DDAB were then constructed for siRNA codelivery for combination therapy. The dual sensitive CPT-PCB/siPlk1 lipoplexes simultaneously delivered the two drugs to tumor cells and enabled a temporally controlled release of two drugs, that the siRNA was quickly released after 4 h incubation due to the protonation of PCB in endosomes/lysosomes, and CPT was released in a sustained manner in response to pH and esterase and highly accumulated in nucleus after 12 h incubation. The CPT-PCB/siPlk1 lipoplexes induced significant cell apoptosis and cytotoxicity *in vitro* with a synergistic effect. Furthermore, the dual sensitive CPT-PCB lipoplexes enhanced the tumor accumulation of the two payloads and exhibited a synergistic tumor suppression effect in tumor-bearing mice *in vivo*, which proved to be a promising delivery system for codelivery of CPT and siPlk1 for cancer therapy.

1. Introduction

The combination of traditional chemotherapy and newly emerging small interfering RNA (siRNA)-based therapy with different mechanisms can cooperatively prohibit cancer development and is a promising strategy for effective treatments of cancers with synergistic or combined effects [1–4]. Camptothecin (CPT) as a traditional chemotherapeutic drug inducing tumor cells apoptosis after binding to DNA topoisomerase I, which has shown a broad spectrum of antitumor activity against various types of malignancies [5–7]. It has been proved that the treatment of tumor cells with siRNA targeting Plk1 could improve the sensitivity of cancer cells to CPT and CPT exerts more cytotoxicity [8,9]. Unfortunately, the intrinsic deficiencies of CPT and siPlk1 such as structural instability, short plasma half-life and lack of tumor target following intravenous administration extremely impeded their clinical application [10–13]. At the same time, it is expected that the chemotherapeutic drug and siRNA should be simultaneously delivered to the same tumoral cell after systemic administration [14,15]. Ideally, the modulator siPlk1 should be released earlier and faster than the chemotherapeutic drug to down-regulate the Plk1 expression in advance and then enhance the tumor cell sensitivity to CPT [16,17]. Therefore, it is urgently needed to develop highly efficient and safe codelivery systems that could temporally controlled release of CPT and siPlk1 for cancer therapy.

To resolve above problems, various nano-sized drug carriers such as liposomes, amphiphilic diblock copolymer micelles and polymers have been constructed to non-covalent encapsulate of these two drugs [18,19]. However, the chemotherapeutic drug contents generally cannot exceed 10% in most of the nano-sized drug carriers to minimize the initial drug release in blood before reaching the tumor target, especially that the CPT undergoes

* Corresponding author. Fax: +86 (0)10 82544853.
** Corresponding author. Fax: +86 371 67781908.
E-mail addresses: zhangzz08@126.com (Z. Zhang), xzhang@home.ipe.ac.cn (X. Zhang).

http://dx.doi.org/10.1016/j.biomaterials.2014.08.022
0142-9612/

lactone ring-opening hydrolysis to form the inactive carboxylate form under physiological condition (pH equal to or above 7) [20–23]. Additionally, hydrophilic polymers were often used to make modification of these nano-sized drug carriers to extend their blood circulation time. However, the steric barrier due to these hydrophilic polymers often interferes with the endosomal/lysosomal escape of the carriers, which resulted in delayed release of siRNA [24–26]. Most importantly, the non-covalent encapsulation could not achieve a temporal release manner and simultaneous release two drugs after endosomal/lysosomal escape.

To circumvent this problem, based on our previous work, we designed a smart zwitterionic polymer poly(carboxybetaine) (PCB)-based pH and esterase-sensitive CPT prodrug, which constructed cationic liposomes with cationic lipid DDAB for siRNA codelivery in a temporally controlled release manner for effective treatment of cancers with combined effects (Scheme 1). First, the CPT-PCB prodrug molecular converted the therapeutic agent CPT into an inactive but more stable prodrug that reverted back to the pharmacologically active moiety triggered by unique biological stimuli of pH and esterase, which could enhance the stability of CPT and delay the CPT release in physiological condition [27]. Second, the CPT-PCB prodrug with balanced amphiphilicity would replace inert molecules of liposomes and enhance the loading content of CPT [28,29]. Third, in our previous study, it has been proved that PCBylation has superior ability in extending the blood retention without interfering with the endosomal/lysosomal escape of siRNA due to the protonation of PCB in acidic condition, which could accelerate the release of siRNA [30]. Therefore, the CPT-PCB prodrug based siPlk1 lipoplexes enabled a temporally controlled release of these two drugs that the siPlk1 was released earlier and faster from the endosomes/lysosomes to cytoplasm due to the protonation of PCB in acidic condition to down-regulate the Plk1 expression in advance, while the conjugated CPT was released in a sustained and pH and esterase-dependent manner and then highly accumulated in nucleus to exert therapeutic effect. It was expected that the CPT-PCB prodrug based siRNA codelivery system could exhibit synergistic actions and has promising application in cancer therapy.

In the following study, anticancer drug CPT was modified with pH-sensitive PCB through ester bond and cationic liposomes with the dual sensitive CPT-PCB prodrug and cationic lipid DDAB were constructed as a carrier of siPlk1 for combination therapy. In order to contrast, DSPE-PCB based cationic liposomes non-covalent encapsulating CPT and non pH-sensitive zwitterionic polymer poly(methacryloyloxyethy phosphorycholine) (PMPC) based CPT prodrug based cationic liposomes as siRNA delivery system under the same condition were also fabricated. The physicochemical properties of the CPT-PCB/siRNA lipoplexes including serum stability, intracellular uptake and endosomal/lysosomal escape were evaluated. Furthermore, the combination of CPT prodrug and siPlk1 for tumor treatment *in vitro* and *in vivo* were investigated.

2. Materials and methods

2.1. Materials

2-Bromoisobutyryl bromide (97%), 2-(*N*,*N*′-dimethylamino)ethyl methacrylate (DMAEMA, 98%), trimethylamine (TEA, 99%) were from Alfa Aesar. β-Propiolactone (98%) and dimethyldioctadecylammonium bromide (DDAB) were purchased from J&K Scientific Ltd. Cholesterol (95%) and 1,2-distearoyl-*sn*-glycero-3-phosphoethanolamine (DSPE) were purchased from Advanced Vehicle Technology Ltd. Co (Shanghai, China). Camptothecin (>99%) was obtained from Melonepharma (Dalian, China). 2-Methacryloyloxyethyl phosphorylcholine (MPC) and 3-(4,5-dimethylthiazol-2-yl)-2,5-diphenyltetrazolium bromide (MTT) were obtained from Sigma–Aldrich. Cy5-siRNA (antisense strand, 5′-UUUGAAGUAUGCCUCAAGGdTdT-3′), FAM-siRNA (antisense strand, 5′-UUUGAAGUAUGCCUCAAGGdTdT-3′), negative control siRNA (siNonsense, antisense strand, 5′-ACGUGACACGUUCGGAGAAdTdT-3′) and siRNA targeting Plk1 mRNA (siPlk1, antisense strand, 5′-UAAGGAGGGUGAUCUUCUUCAdTdT-3′) were synthesized by Su-zhou Ribo Life Science Co. (Kunshan, China).

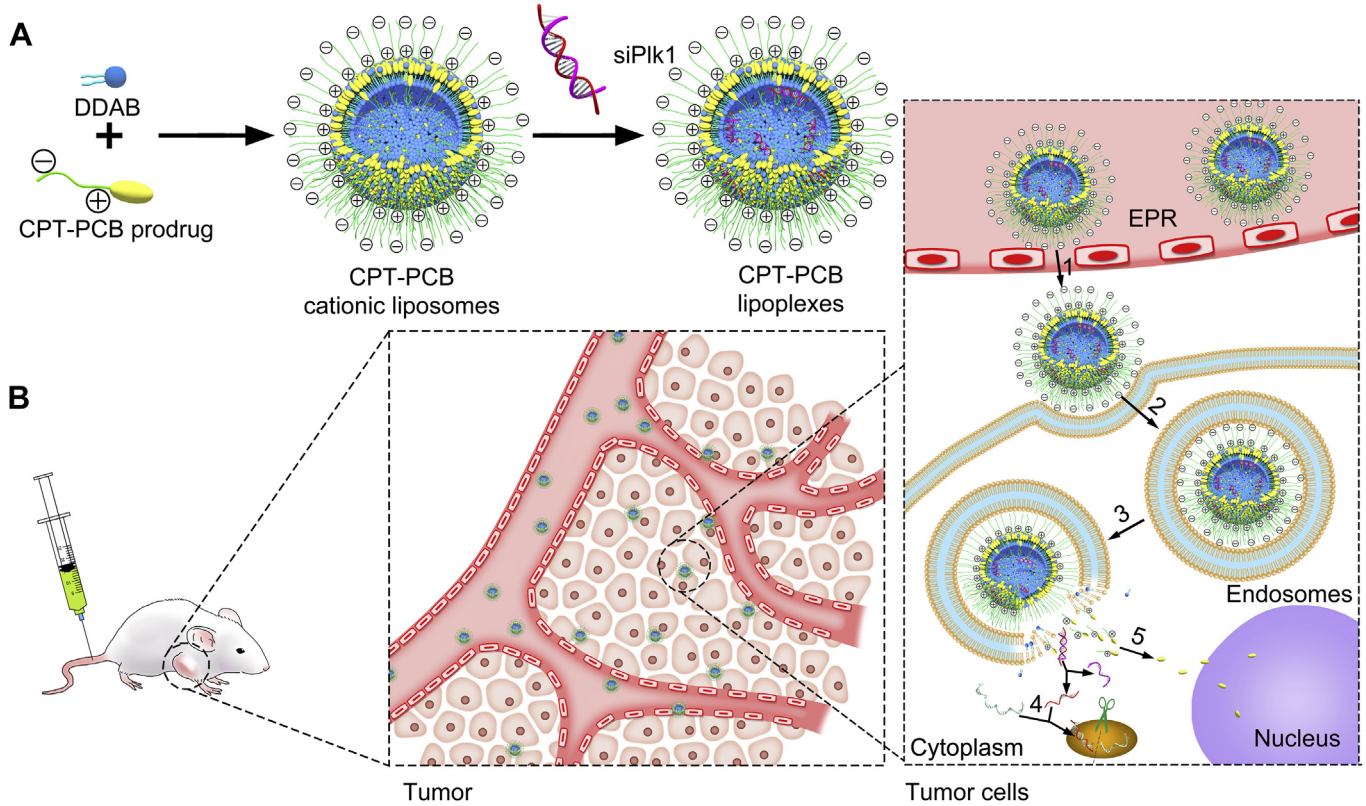

Scheme 1. Schematic illustrations of (A) the formation of CPT-PCB cationic liposomes and lipoplexes and (B) cellular uptake and subcellular drug release behaviors of CPT-PCB lipoplexes.

2.2. Sample synthesis

2.2.1. Synthesis and purification of CB monomer

CB was synthesized according to the method reported before [30]. Briefly, β-propiolactone (0.43 g, 6 mmol) in 5 mL of dried dichloromethane was added dropwise to 25 mL of dried dichloromethane containing DMAEMA (0.79 g, 5 mmol). The reaction mixture was stirred under nitrogen protection at 10 °C for 12 h. The white precipitate was washed with 50 mL of dried dichloromethane and 50 mL of anhydrous acetone. The product was then dried under reduced pressure to obtain the final CB. ^{1}H NMR (300 MHz, D_2O): δ 6.06 (s, 1H, −C*H*═CCH$_3$−), 5.85 (s, 1H, −C*H*═CCH$_3$−), 4.58 (m, 2H, −OC*H*$_2$CH$_2$N−), 3.70 (m, 2H, −OCH$_2$C*H*$_2$N−), 3.59 (t, 2H, −NC*H*$_2$CH$_2$COO−), 3.10 (s, 6H, −NCH$_3$C*H*$_3$−), 2.64 (t, 2H, −NCH$_2$C*H*$_2$COO−), 1.84 (s, 3H, CH$_2$═CC*H*$_3$−).

2.2.2. Synthesis and purification of CPT-Br initiator

CPT (300 mg, 0.86 mmol) was suspended in 20 mL of dried dichloromethane with 0.2 mL of triethylamine (0.2 mL, 1.6 mmol). After the suspension was cooled to 0 °C, 2-bromopropionyl bromide (372 mg, 1.72 mmol) in 5 mL of dried dichloromethane was added to the suspension. The reaction mixture was stirred at 0 °C for 1 h, then at room temperature for 4 h. After washing with 1N HCl, 1% $NaHCO_3$ and brine, the organic phase was dried over Na_2SO_4. The Na_2SO_4 was filtered and the organic phase was concentrated by rotary evaporation to give the crude product. The crude product was crystallized in CH_3OH/CH_2Cl_2 (volume ratio 95:5) to obtain the final product. ^{1}H NMR (300 MHz, $CDCl_3$): δ 8.44 (s, 1H, −C−C*H*−C−), 8.29 (d, 1H, −CH−C*H*−C−), 7.97 (d, 1H, −CH−C*H*−C−), 7.86 (t, 1H, −CH−C*H*−CH−), 7.70 (t, 1H, −CH−C*H*−CH−), 7.52 (s, 1H, −C−C*H*−C−), 5.73 (d, 1H, −C−C*H*−O−), 5.43 (d, 1H, −C−C*H*−O−), 5.32 (s, 2H, −C−C*H*$_2$−N−), 4.62 (q, 1H, −CO−C*H*−CH$_3$), 2.16–2.41 (m, 2H, −C−C*H*$_2$−CH$_3$), 1.86 (d, 3H, −CH−C*H*$_3$), 1.03 (t, 3H, −CH$_2$−C*H*$_3$) [31].

2.2.3. Synthesis and purification of CPT-PCB$_n$ polymers

CPT-PCB$_n$ was synthesized by the ATRP using CPT-Br as the initiator. A typical synthesis procedure with the theoretical degree of polymerization (DP) of 20 was described as follows. CPT-Br (9.66 mg, 0.02 mmol) was dissolved in 5 mL of dichloromethane, and CB (91.71 mg, 0.40 mmol) monomer was dissolved in 10 mL of ethanol. CPT-Br, CB and CuBr (5.74 mg, 0.04 mmol) were added to a clean and dry schlenk flask. The schlenk flask was degassed by three freeze-pump-thaw cycles and recharged with nitrogen. PMDETA (6.93 mg, 0.04 mmol) dissolved in 1 mL of ethanol was injected into the frozen system. The schlenk flask was stirred for 24 h at 60 °C. The impurities and unreacted monomers were removed by dialyzing in a Cellu SepH1-membrane (MWCO3500) against ethanol and deionized water for 48 h, respectively, and lyophilized to obtain the final product. ^{1}H NMR (300 MHz, $CDCl_3$): δ 4.10 (m, 2H, −OC*H*$_2$CH$_2$N−), 4.02 (m, 2H, −OCH$_2$C*H*$_2$N−), 3.25 (m, 2H, −NC*H*$_2$CH$_2$COO−), 2.60 (m, 2H, −NCH$_2$C*H*$_2$COO−), 2.25 (m, 6H, −NC*H*$_3$C*H*$_3$−), 1.80 (m, 2H, −BrCC*H*$_2$CH$_3$), 1.00 (m, 3H, −BrCC*H*$_3$−). CPT-PMPC$_n$ with the same theoretical DP was prepared in a similar way. ^{1}H NMR (300 MHz, CD_3OD): δ 4.30 (m, 2H, −OC*H*$_2$CH$_2$O−), 4.10 (m, 2H, −OC*H*$_2$CH$_2$N−), 4.00 (m, 2H, −OCH$_2$C*H*$_2$O−), 3.60 (m, 2H, −OCH$_2$C*H*$_2$N−), 3.22 (m, 9H, −N(C*H*$_3$)$_3$), 1.80 (m, 2H, −BrCC*H*$_2$CH$_3$), 1.00 (m, 3H, −BrCC*H*$_3$−) [31]. DSPE-PCB$_n$ polymer with the same DP was synthesized according to the method we reported before [30].

The structure of all the products was characterized by ^{1}H NMR spectra recorded on a Bruker 300 MHz spectrometer. The degree of polymerization of CPT-PCB$_n$, CPT-PMPC$_n$ and DSPE-PCB$_n$ was confirmed by ^{1}H NMR spectra. The structure or degree of polymerization of CPT-Br, CPT-PCB$_n$ and CPT-PMPC$_n$ were also measured by the adsorption of CPT at the wavelength of 366 nm on a UV-spectrophotometer (TU-1810, Beijing, China). The calibration curves were generated using known concentrations of CPT.

The critical vesicle formation concentration (CV_fC) was determined by fluorescence method using nile red as a hydrophobic fluorescent probe. Nile red with the final concentration of 1×10^{-6} mol/L in CH_2Cl_2 was added to a series of vials and the CH_2Cl_2 was evaporated under reduced pressure. A measured amount of CPT-PCB$_n$ with different DPs was added to each vial. PBS (pH = 7.4) was added to the vials to obtain CPT-PCB$_n$ concentrations ranging from 5×10^{-4} to 2 mg/mL. The vials were stirred at 37 °C overnight, and then the fluorescence intensity was measured using a

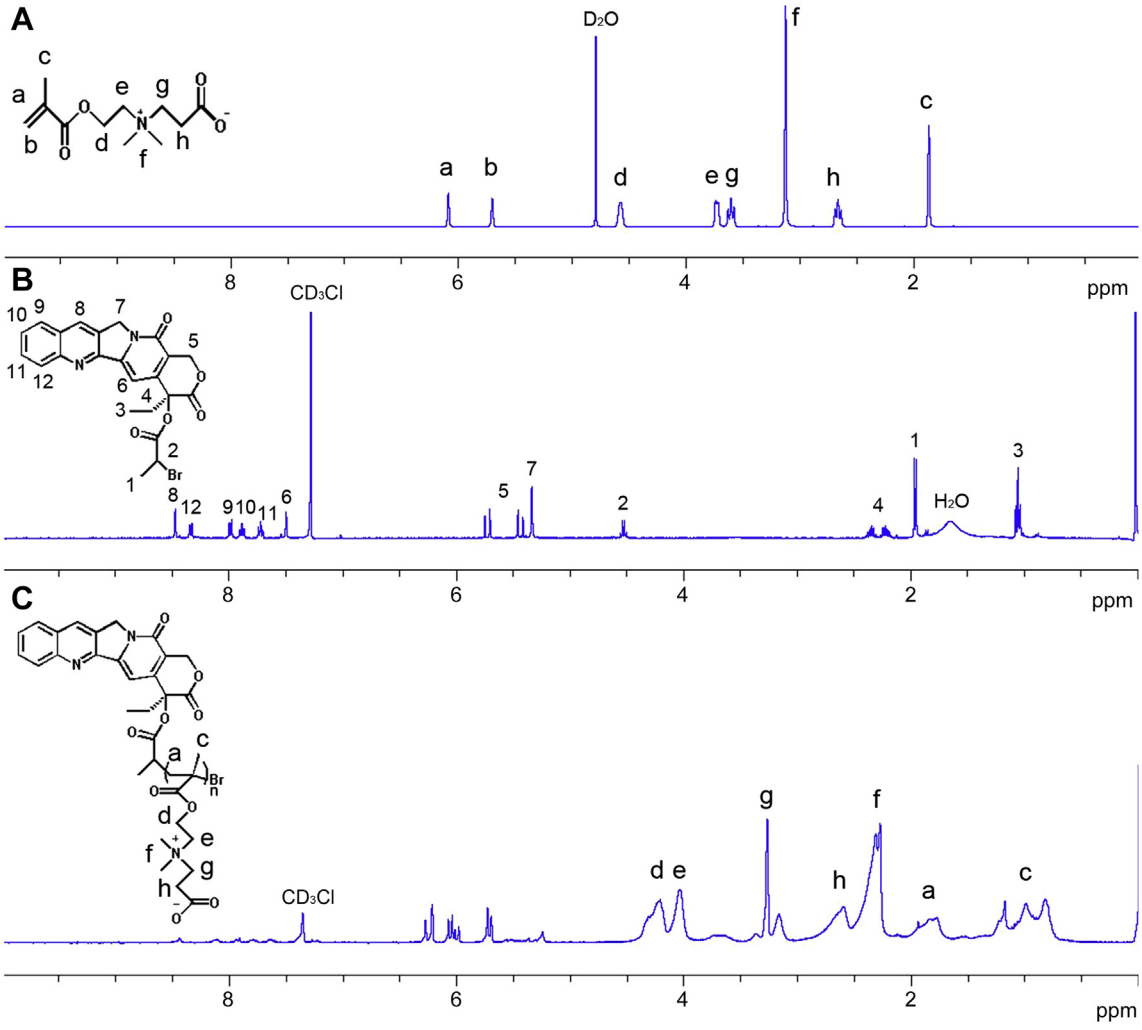

Fig. 1. ^{1}H NMR spectra recorded for (A) CB monomer. (B) CPT-Br initiator. (C) CPT-PCB$_6$ polymer.

Table 1
Characterization of CPT-based products by UV-spectrophotometer.

Theory	DPs	CPT/polymer (%)	Theoretical value (%)
CPT-Br		73.1 ± 3.3	72.1
CPT-PCB_{10}	3	33.9 ± 1.8	33.6
CPT-PCB_{20}	6	22.9 ± 3.5	20.2
CPT-PCB_{40}	13	9.2 ± 3.9	10.4

microplate reader (SpectraMax M5, Molecular Devices, CA, USA) with the excitation wavelength of 485 nm and emission wavelength of 525 nm. The CV_fC was obtained as the intersection of the tangents to the two linear portions of the fluorescence intensity as a function of CPT-PCB_n concentration.

2.3. Preparation of CPT-PCB_n based liposomes and lipoplexes

CPT-PCB_n based cationic liposomes were prepared by thin lipid film method. Briefly, DDAB and CPT-PCB_n with different molar ratio were dissolved in chloroform. The organic phase was removed at 55 °C on a rotary evaporator to obtain a thin lipid film. The lipid film was hydrated with 10 mL of PBS. After sonication at 37 °C for 30 min, the solution was extruded 5 times using EmulsiFlex-C5 high-pressure homogenizer (Avestin, Canada). Liposomes with DSPE-PCB_n encapsulating CPT or CPT-$PMPC_n$ were also prepared by the same way. Unencapsulated CPT for DSPE-PCB_n liposomes was removed by Sephadex G75 size exclusion chromatography. Lipoplexes were prepared by mixing cationic liposomes and siRNA at designed N/P ratio for 30 min at room temperature. The mean diameter of cationic liposomes and lipoplexes was measured by dynamic light scattering (DLS), and the zeta potential was analyzed using a Zetasizer Nano ZS instrument (Malvern Instruments). Further morphological analysis was carried out by transmission electron microscopy (H-7650 TEM, Japan) using negative staining with 1% phosphotungstic acid (PTA) and cryogenic transmission electron microscopy (Cryo-TEM, FEI Tecnai 20, Netherlands).

2.4. The encapsulation efficiency and loading content of CPT and siRNA

The encapsulation efficiency and loading content of CPT were determined using UV-spectrophotometer at the wavelength of 366 nm. The drug encapsulation efficiency and loading content were calculated as follows:

$$\text{Encapsulation efficiency}(\%) = W_2/W_1 \times 100\%$$

$$\text{Drug loading content}(\%) = W_2/W_0 \times 100\%$$

where W_2 was the weight of CPT in liposomes, W_1 was the weight of CPT used for encapsulating and W_0 was the weight of total liposomes.

To evaluate the efficiency of siRNA encapsulated in cationic liposomes, the fluorescence of unencapsulated siRNA was measured by Quant-iT™ RiboGreen® RNA Reagent (Invitrogen). After centrifugation at 5000 × *g* for 5 min, the amount of siRNA in supernatant was measured. For the low-range assay, 100 μL of the reagent was added to microplate wells and the samples were quantified using microplate reader with the excitation wavelength of 485 nm and emission wavelength of 530 nm. The encapsulation efficiency of siRNA was calculated using the formula:

$$\text{Encapsulation efficiency}(\%) = (F_0 - F_1)/F_0 \times 100\%$$

where F_0 was the fluorescence of siRNA used for encapsulation, F_1 was the fluorescence of siRNA in supernatant.

2.5. Serum stability of lipoplexes

For investigation of serum stability, the lipoplexes at a concentration of 1 mg/mL were incubated in DMEM containing 10% FBS at 37 °C under gentle stirring. At each time point, the mean diameters of the lipoplexes were calculated in triplicate using DLS.

2.6. Release of CPT from lipoplexes

The *in vitro* release of CPT was performed in PBs with different pH values (3.5, 5.0 and 7.4) and pH 7.4 with esterase in a time-course procedure. CPT was isolated by dialysis bag (MWCO 3500, Millipore). The CPT concentration in solution was detected using high performance liquid chromatography (HPLC) equipped with a UV detector and a Phenomenex C_{18} column at 25 °C (Shimadzu, Japan). The mobile phase was acetonitrile and water (volume ratio 50:50, Merck LiChrosolv, HPLC grade) at a flow rate of 1.0 mL/min and a UV detector at 366 nm wavelength. The free CPT was determined based on the peak area at the retention time of 4.8 min according to the calibration curve. The release percentage of CPT was calculated using the formula:

$$\text{Release percentage}(\%) = W_1/W_0 \times 100\%$$

where W_1 was the weight of CPT in solution, W_0 was the weight of total CPT in liposomes.

2.7. pH-sensibility of PCB modified liposomes

The buffering capacity of PCB or PMPC modified CPT lipoplexes was determined by acid-base titration. Briefly, PCB or PMPC modified CPT-based lipoplexes were dissolved in 0.01 M NaCl and the solution was adjusted to pH 10 with 1 M NaOH. The solution was titrated by the stepwise addition of 0.1 M HCl to obtain the titration profile. To measure the pH-sensibility of PCB modified lipoplexes, lipoplexes were incubated in phosphate buffer (PB) solution of different pH at 37 °C for 30 min. The zeta potential of the lipoplexes was measured with a Zetasizer Nano ZS instrument.

2.8. Flow cytometry and confocal laser scanning microscopy measurement

Briefly, Hela cells were seeded in 12-well plates at 1×10^5 cells/well in 800 μL of culture medium for 24 h. The cells were then incubated with lipoplexes containing 1 μg of FAM-siRNA in DMEM with 10% FBS medium. After 2 h of incubation, the cells were rinsed three times with cold PBS, trypsinized and harvested in PBS. Then the samples were assessed with BD Calibur flow cytometry (BD Co., USA) to determine the fluorescence intensity of FAM-siRNA (488 nm) and CPT (405 nm).

To elucidate the mechanisms underlying the cellular internalization of different modification lipoplexes, the cellular uptake studies were performed at 4 °C or in the presence of various endocytic inhibitors for 2 h. Briefly, prior to the addition of lipoplexes, Hela cells were preincubated with endocytic inhibitors including genistein (100 μg/mL), methyl-β-cyclodextrin (mβCD, 50 μM), chlorpromazine (10 μg/mL), dynasore (10 μg/mL) and wortmannin (100 μg/mL) for 30 min. The cells were then incubated with lipoplexes for 2 h at 37 °C. Results were expressed as the uptake percentage of control cells that were only incubated with lipoplexes at 37 °C for 2 h.

To measure the endosomal/lysosomal escape, Hela cells were incubated with lipoplexes including 1 μg of FAM-siRNA for 2 h and 4 h at 37 °C, respectively. The cells were washed three times with PBS and followed by staining with LysoTracker Red for 20 min at 37 °C. The cells were then washed three times with PBS and fixed with 4% paraformaldehyde for 10 min. Nucleus was stained with DAPI for 10 min. The cellular localization was visualized under confocal laser scanning microscopy (CLSM, Zeiss Co., Germany). To further detect the entry of CPT to nucleus, Hela cells were incubated with lipoplexes including 1 μg of FAM-siRNA for 4 h and 12 h at 37 °C, respectively. The cells were then washed three times with PBS and visualized under CLSM.

2.9. In vitro gene silencing efficiency

Hela cells (5×10^5) were seeded in 6-well plates and incubated at 37 °C in 5% CO_2 for 24 h to reach about 70% confluence. Various liposomal formulations were added to 1.5 mL of DMEM with 10% FBS medium and then incubated with the cells for 24 h (for mRNA isolation) or 48 h (for protein extraction). The cellular levels of Plk1 mRNA and protein were assessed using quantitative real-time PCR (qRT-PCR) and western blot (WB), respectively.

2.10. Cytotoxicity and cell apoptosis measurement

To determine the cytotoxicity of the lipoplexes, lipoplexes with various concentration of siRNA were added to 100 μL of the culture medium. The concentration of free CPT was equal to the concentration of CPT for CPT-PCB_6 lipoplexes corresponding to each siRNA concentration. After 72 h incubation, 20 μL of the MTT solution (5 mg/mL in PBS) was added to each well and incubated for additional 2 h. The medium and MTT were then replaced with 100 μL of DMSO. The absorbance was measured at 490 nm using a Tecan microplate reader (Tecan, Switzerland). Untreated Hela cells were used as a negative control and its cell viability was defined as 100%.

For apoptosis analysis, Hela cells (5×10^4) cultured in 24-wells plates were treated with the above-mentioned formulations at the siRNA concentration of 2 μg/mL or free CPT dose of 2.5 μg/mL. After 48 h of treatment, apoptosis cells were detected on BD Calibur flow cytometry (BD Co., USA) using the Annexin V-FITC Apoptosis Detection Kit I (Invitrogen).

2.11. Pharmacokinetics profiles of CPT

ICR mice were randomly divided into 5 groups. All procedures involving experimental animals were performed in accordance with protocols approved by the Institutional Animal Care and Use Committee of Peking University. To determine the pharmacokinetics of CPT with various formulations, free CPT or CPT-based lipoplexes at a dose of 4 mg CPT/kg were administered to mice *via* the tail vein. At the time point of 5 min, 30 min, 2 h, 4 h, 6 h, 8 h and 24 h following injection, blood samples were collected *via* eye puncture. Blood samples were centrifuged at 4000 rpm for 10 min to obtain the plasma and the CPT was extracted with methanol. The concentration of CPT was detected using microplate reader with the excitation wavelength of 366 nm and emission wavelength of 450 nm.

2.12. In vivo distribution study in tumor-bearing mice

Six weeks old Hela-bearing nude mice, with body weight between 18 and 22 g, were purchased from the Academy of Military Medical Sciences of China. Lipoplexes with Cy5-siRNA were administered to each mouse *via* tail vein injection at 2.0 mg Cy5-siRNA/kg. Free CPT was administered to each mouse at 2.5 mg/kg. At designed time point, mice were sacrificed, and the tissue samples were harvested and

examined with a Kodak *in vivo* imaging system (Kodak In-Vivo Imaging System FX Pro. Carestream Health, USA). The tissue samples were then grinded and CPT was extracted with methanol. The concentration of CPT was determined using microplate reader. Part of the tumor tissues were then cross-sectioned using a vibration microtome. The nucleus of the tissue cells was stained using DAPI solution. Samples were observed under CLSM (Zeiss Co., Germany).

2.13. *In vivo antitumor activity evaluation*

In order to evaluate the antitumor activity of CPT-PCB_n based lipoplexes, Hela tumor-bearing mice were randomly divided into different groups, and treated with various formulations *via* tail vein injection every other day. The doses of lipoplexes with siPlk1 or siNonsense of each injection were fixed at 2 mg/kg. The dose of free

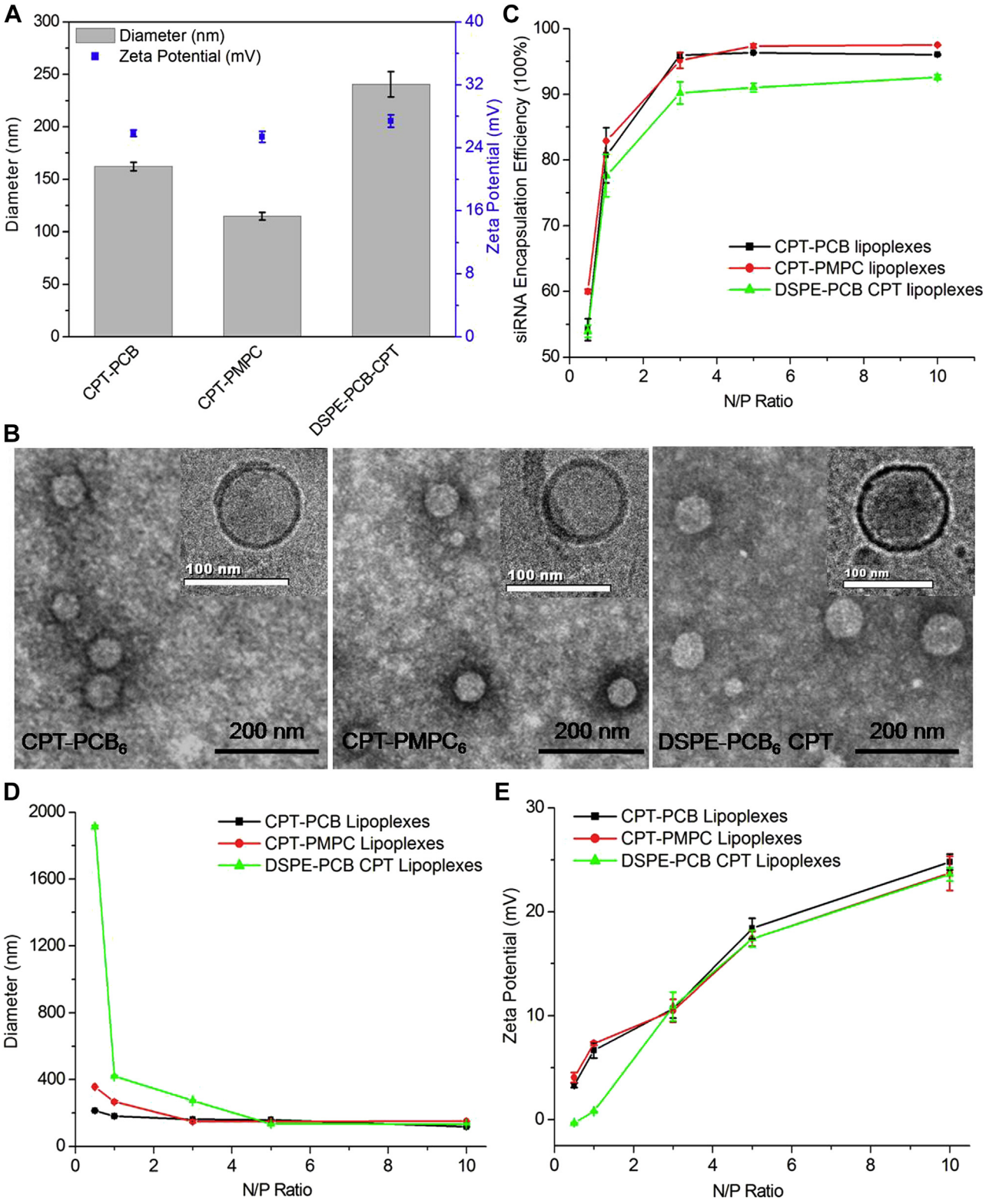

Fig. 2. The characterization of cationic liposomes and lipoplexes. (A) The diameter and zeta potential of CPT-based cationic liposomes. (B) The TEM and Cryo-TEM images of CPT-based cationic liposomes. (C) The siRNA encapsulation efficiency of lipoplexes. (D) Changes of diameters of lipoplexes with a function of N/P ratio. (E) Changes of zeta potential of lipoplexes with a function of N/P ratio.

Table 2
The CPT loading content and encapsulation efficiency of cationic liposomes with molar ratio of 3:7.

Liposomes 3:7	Drug loading (%)	Encapsulation efficiency (%)
CPT-PCB_6	21.0 ± 5.6	
CPT-$PMPC_6$	15.4 ± 1.9	
DSPE-PCB_6 CPT	9.0 ± 0.8	65.5 ± 2.9

CPT was 2.5 mg/kg. The tumor volume and the body weight of the mice were measured every other day. The tumor volume was measured using the formula:

$$V\left(\mathrm{mm}^3\right) = \left(a \times b^2\right)/2$$

where a and b are the major and minor axes of the tumor, respectively.

At 24 h post-injection, the mice were sacrificed and the main organs and tumor were harvested from the animals. The level of Plk1 mRNA and protein in tumor tissue was analyzed by qRT-PCR and WB as the method described above. The cell apoptosis of tumor tissue was detected by the terminal deoxynucleotidyl transferase dUTP nick end labeling (TUNEL) assay according to the manufacturer's protocol (Vazyme™). The cell nucleus was stained by DAPI and the samples were analyzed under fluorescence microscopy (Nikon, Japan).

2.14. Statistical analysis

The data is summarized as the mean value with standard deviation of triplicate measurement. Unpaired student's *t*-test was used to assess statistical differences ($p < 0.05$) between the group means. All experiments were done in triplicate with a minimum of three independent experiments.

3. Results and discussion

3.1. Synthesis and characterization of CPT-PCB_n prodrug polymers

The CPT-based prodrug polymer CPT-PCB_n was synthesized *via* ATRP using CPT-Br as the initiator (Supporting Information, Scheme S1). The CPT-PCB_n with different DPs was achieved by adjusting the ratio of initiator CPT-Br and monomer CB. The structures of the monomer, initiator and polymers have been confirmed by ^{1}H NMR (Fig. 1). The lactone ring structure of CPT was retained in the CPT-Br and CPT-PCB_n polymers as also confirmed by ^{1}H NMR. By calculating the integral ratio of CPT protons to the monomer CB protons in the ^{1}H NMR, the DPs of CPT-PCB_n were determined to be 3, 6 and 13 with the theoretical values of 10, 20 and 40, respectively (Table 1). The ratios of CPT to polymers with different DPs were calculated by UV-spectrophotometer at the wavelength of 366 nm. The ratio of CPT in CPT-Br initiator was 73.1%, which accorded well with the theoretical value of 72.1%. The ratios of CPT-PCB_n polymers with DPs of 3, 6 and 13 were 33.9%, 22.9% and 9.2%, respectively, which were also in line with their theoretical values. As expected, the CPT loading content of CPT-PCB_n was decreased with the increase of DP.

The CV_fC of CPT-PCB_n polymers were obtained using nile red fluorescence method. The CPT-PCB_3, CPT-PCB_6 and CPT-PCB_{13} polymers formed nano-sized particles with the CV_fC of 20, 26 and 49 μg/mL, respectively (Supporting Information, Fig. S3). The CV_fC of CPT-PCB_{13} was higher than that of CPT-PCB_3 and CPT-PCB_6 as it had a low fraction of the hydrophobic part. With higher fraction of hydrophobic part, the liposomes made from CPT-PCB_3 were easily precipitated (data not shown). This was probably because the amphiphilicity of CPT-PCB_3 was not balanced to form liposomes. Therefore, with excellent CPT loading content and amphiphilic balance, the following studies were focused on the CPT-PCB_6 based prodrug system.

In order to contrast, zwitterionic polymer PMPC modified CPT-$PMPC_6$ prodrug polymer was also synthesized *via* ATRP (Supporting Information, Fig. S1). The structure of the polymer has been confirmed by ^{1}H NMR (Supporting Information, Fig. S2) and the CPT loading content was 16.4% as calculated by UV-spectrophotometer.

3.2. Preparation and characterization of CPT-based liposomes and lipoplexes

CPT prodrug based cationic liposomes were prepared by thin lipid film method and the cationic liposomes served as carriers of siPlk1 for combination therapy. The size and surface property are important physiochemical parameters for the delivery system [32]. The diameters of cationic liposomes with the DDAB and CPT-PCB_6 molar ratio of 9:1 and 8:2 were larger than 250 nm and were tended to precipitate (Supporting Information, Fig. S4). This was probably because that the large repulsive force destabilized the liposomes with high molar ratio of DDAB. The diameters of cationic liposomes with DDAB and CPT-PCB_6 molar ratio of 7:3 to 2:8 were similar in a range of 100–200 nm, which was favorable for tumor accumulation *via* the enhanced permeability and retention (EPR) effect [33]. As expected, the zeta potential of cationic liposomes was decreased with the decreased molar ratio of DDAB. At molar ratio of 2:8, the zeta potential was approximately neutral, which was not favorable for siRNA complexing. At the same time, the CPT loading content was increased with the decreased molar ratio of DDAB. With excellent drugs loading ability, cationic liposomes with the molar ratio of 3:7 of DDAB and CPT-PCB_6 were the ideal system for CPT and siRNA combination therapy and were chosen for the following experiments.

In order to contrast, DSPE-PCB_6 cationic liposomes encapsulating CPT or CPT-$PMPC_6$ prodrug polymer based cationic liposomes with the lipid molar ratio of 3:7 were also prepared by the same way. As shown in Fig. 2A, all zwitterionic polymer modified CPT cationic liposomes had comparable positive surface charge, of about 25.0 mV. However, the diameter of DSPE-PCB_6 CPT cationic liposomes was much larger than that of CPT prodrug system due to their non-covalent encapsulation of CPT. All the CPT-based cationic liposomes had spherical shape as confirmed by TEM and Cryo-TEM (Fig. 2B).

The loading content of CPT for CPT-PCB_6 prodrug cationic liposomes was 21.0%, which was about 2.3 times of that for DSPE-PCB_6 CPT cationic liposomes (9.0%) as the hydrophobic CPT replacing the

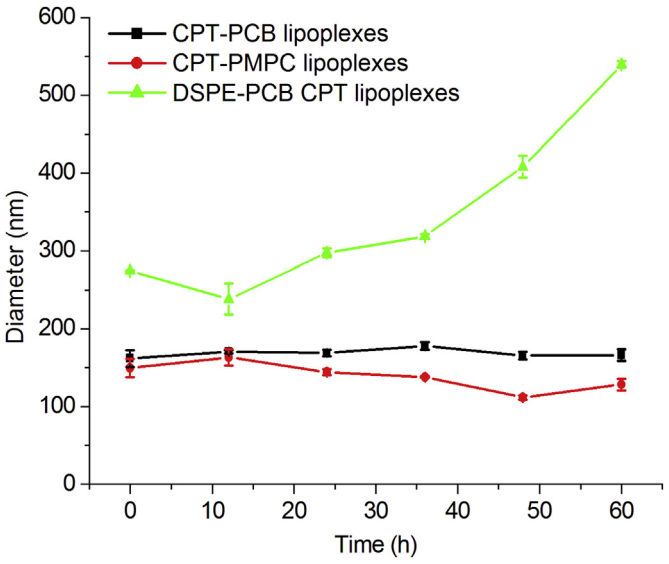

Fig. 3. Changes in particle sizes of the CPT-based lipoplexes as a function of incubation time with 10% FBS at 37 °C. Data are shown as the mean ± S.D. of three independent experiments.

inert DSPE for PCB modification (Table 2). The higher drug loading content could reduce the administrating doses of CPT as high dose of excipient might cause systemic toxicity and impose an extra burden for the patients to excrete the carriers.

It was very important to selective an appropriate N/P ratio of lipoplexes for *in vitro* and *in vivo* application. The siRNA encapsulation efficiency was measured using Quant-iT™ RiboGreen® RNA Reagent. As shown in Fig. 2C, there was no remarkable difference in siRNA encapsulation efficiency for those three cationic liposomes and the encapsulation efficiency obviously increased with the increase of N/P ratio from 0.5 to 3, about 50%–90%. However, there was no obviously increment when the N/P increased from 3 to 10. Although excess cationic liposomes decreased the diameter of the lipoplexes, the excess cationic lipid enhanced the surface positive charge of the lipoplexes, which had negative effect on the serum stability (Fig. 2D and E). Therefore, lipoplexes with N/P ratio of 3 were chosen for the following experiments.

3.3. Stability of the lipoplexes

Zwitterionic polymer could resist nonspecific protein adsorption to enhance the stability of lipoplexes. To evaluate the serum stability of the CPT-based lipoplexes with different formulation, the average particle diameters of the lipoplexes in 10% FBS were measured at designed time point. As shown in Fig. 3, only slight increment of diameters after 60 h incubation was observed for CPT-PCB_6 and CPT-$PMPC_6$ based lipoplexes. However, the diameter of CPT encapsulated delivery system DSPE-PCB_6 CPT lipoplexes was increased from 274.4 nm to 539.7 nm after incubation. The increment was probably due to the accelerated CPT release behavior in physiological condition for CPT non-covalent encapsulated nanoparticles.

3.4. CPT release from CPT-based cationic liposomes in different pH medium in vitro

The CPT-based cationic liposomes were expected to enable a temporal release of the two payloads: siPlk1 was fast released to cytoplasm to down-regulate the Plk1 expression in advance, and CPT was released in a sustained manner in response to pH and esterase. To demonstrate this potential, the release kinetic of CPT in medium with pH of 7.4, 5.0, 3.5 or esterase at 37 °C was quantified. The DSPE-PCB_6 CPT encapsulating system exhibited rapid drug release rates for around 50% in the initial 10 h at pH 7.4, which might induce the initial drug release in the blood before reaching the tumor target and limit its application in tumor therapy (Fig. 4A). Notably, the release profiles showed that no significant initial burst release could be observed in pH 7.4 medium for CPT-PCB_6 prodrug based lipoplexes, while the CPT

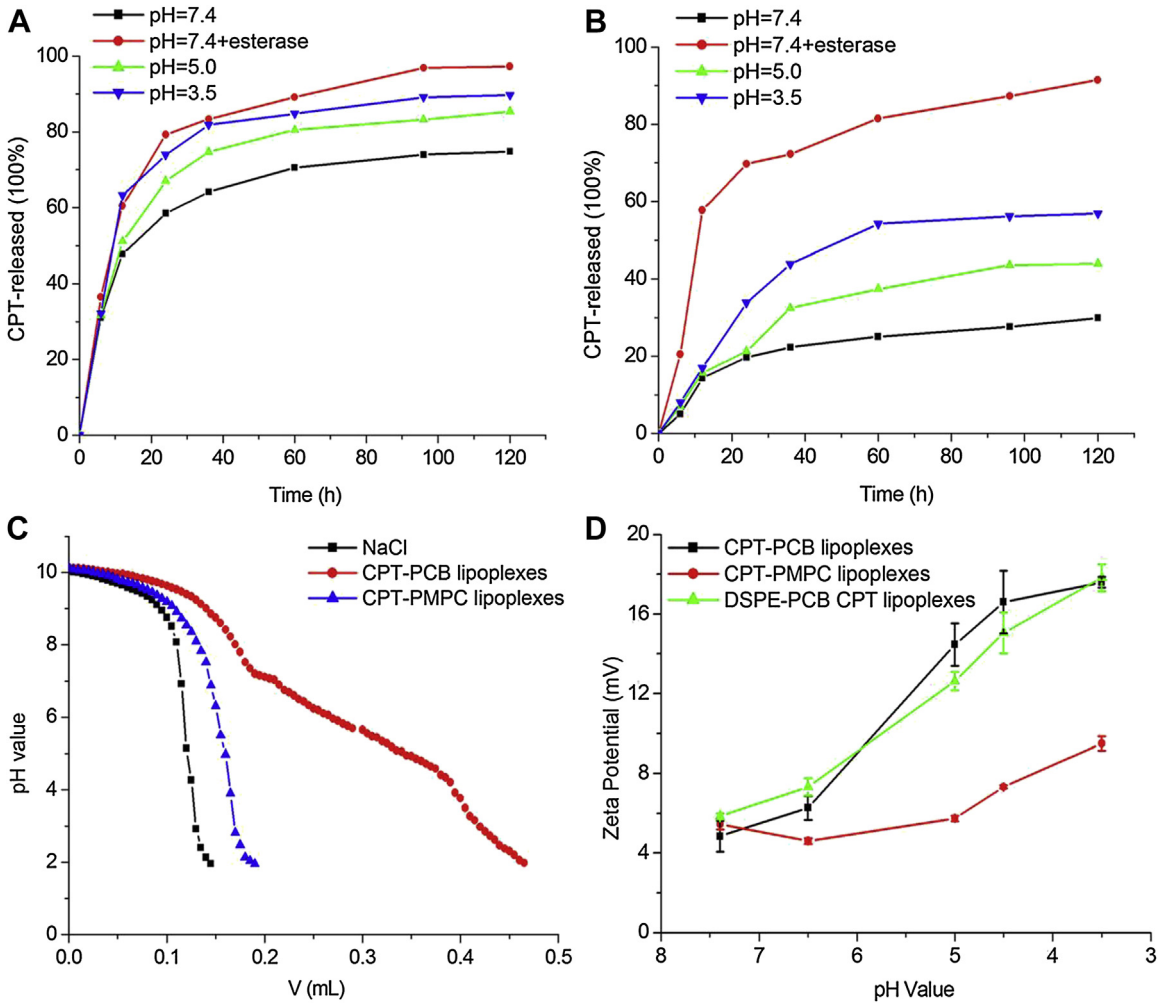

Fig. 4. The CPT release profiles for (A) DSPE-PCB_6 CPT lipoplexes. (B) CPT-PCB_6 lipoplexes at pH of 7.4, 5.0, 3.5 and 7.4 with esterase at 37 °C. The concentration of CPT was detected using HPLC. (C) The buffering capacity of PCB and PMPC modified CPT lipoplexes detected by acid-base titration. (D) Changes of zeta potential of lipoplexes as a function of pH values. Data are shown as the mean ± S.D. of three independent experiments.

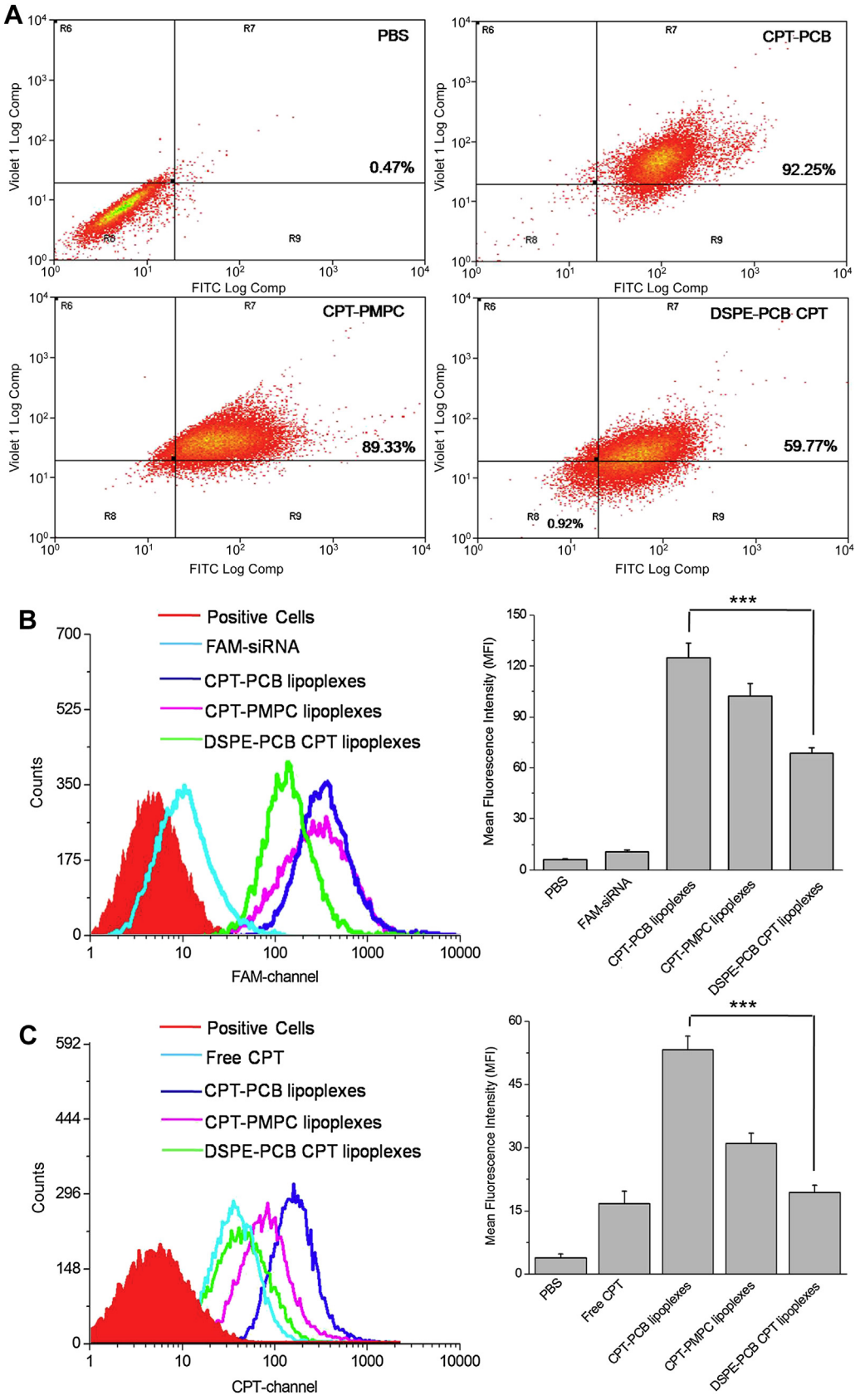

Fig. 5. Cellular uptake of CPT-PCB_6, CPT-$PMPC_6$ and DSPE-PCB_6 CPT lipoplexes with FAM-siRNA in Hela cells after 2 h of incubation at 37 °C. The concentration of FAM-siRNA was 1 μg/mL. The fluorescence intensity was detected by flow cytometry. (A) Co-delivery of CPT-PCB_6, CPT-$PMPC_6$ and DSPE-PCB_6 CPT lipoplexes with FAM-siRNA in Hela cells. (B) Flow cytometric analyses of FAM-siRNA and the mean fluorescence intensity of FAM-siRNA. (C) Flow cytometric analyses of CPT and the mean fluorescence intensity of CPT. Data are shown as the mean ± S.D. of three independent experiments. $^{*}P < 0.05$, $^{**}P < 0.01$, $^{***}P < 0.005$ ($n = 3$).

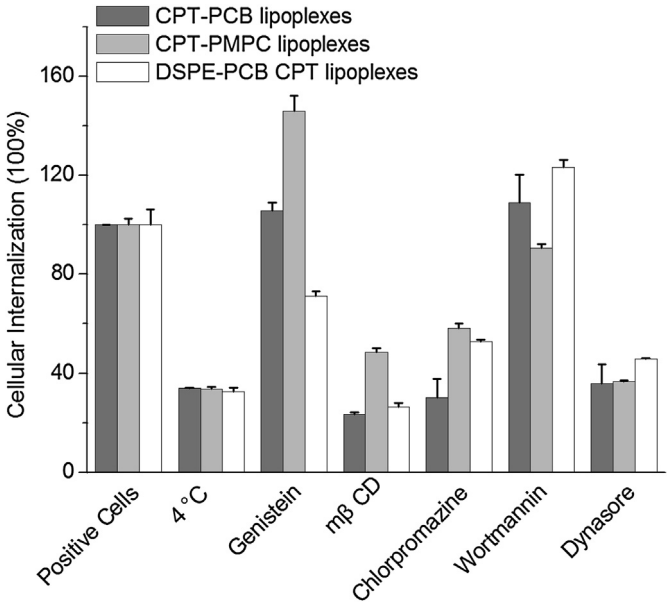

Fig. 6. Mechanistic probes of the intracellular kinetics of the CPT-PCB_6, CPT-$PMPC_6$ and DSPE-PCB_6 CPT lipoplexes in Hela cells by monitoring the cellular uptake level at 4 °C or in the presence of various endocytic inhibitors. Data are shown as the mean ± S.D. of three independent experiments.

release rate was increased with the decrease of pH, and about 56.8% was released from the lipoplexes within 120 h incubation at pH 3.5 in a sustained manner (Fig. 4B). At the same time, the release rate was accelerated after adding esterase, which is abundant in cells [34]. The pH and esterase triggered release behavior of CPT from prodrug system showed great potential in tumor therapy due to its sustained release of CPT in cancer cells while preventing premature drug release following intravenous injection.

3.5. pH sensibility of PCB modified liposomes

It is well known that high buffering capacity of non-viral vectors may play an important role in gene silencing efficiency of lipoplexes because they could be protonized in endosomes/lysosomes and facilitate the endosomal/lysosomal escape of siRNA into the cytoplasm [35,36]. The buffering capacity of PCB or PMPC modified liposomes was investigated by acid-base titration in 0.01 M NaCl aqueous solution. As shown in Fig. 4C, PCB modified liposomes exhibited good buffering capacity over the pH range of 7.4 to 3.5, whereas PMPC modified liposomes had no buffering capacity over the pH range studied. The zeta potential of lipoplexes in different pH condition was further detected to confirm the protonation of PCB (Fig. 4D). The pH value was consistent with the pH from physiological condition to lysosomes [37]. The PCB lipoplexes showed a pH-dependent zeta potential, and enhanced from 4.85 mV at pH 7.4–17.6 mV at pH 3.5 for CPT-PCB_6 prodrug system. The DSPE-PCB_6 CPT lipoplexes also showed the same trend. It meant that the carboxylic acid group of PCB could be protonation in acidic condition and the protonation enhanced the surface charge of PCB-based drug delivery system. While the zeta potential of PMPC modified lipoplexes had no significant change over the pH range studied, which was consistent with the buffer capacity results.

3.6. Cellular uptake of the lipoplexes

The combination of CPT with different mechanism antitumor drug siPlk1 could cooperatively inhibit tumor cells. The simultaneous delivery of CPT and siRNA for lipoplexes was analyzed using flow cytometry. Cells were mainly located in the double-positive quadrant after 2 h of incubation, indicating the lipoplexes indeed delivered two payloads into the cells simultaneously (Fig. 5A). As shown in Fig. 5B, the cellular uptake of CPT-PCB_6 and CPT-$PMPC_6$ lipoplexes was much higher than that of DSPE-PCB_6 CPT lipoplexes due to their excellent serum stability. As expected, the fluorescence intensity of CPT for CPT-PCB_6 lipoplexes was about 3 times of that for CPT non-covalent encapsulated DSPE-PCB_6 lipoplexes due to their higher CPT loading content, which was preferable for antitumor therapy (Fig. 5C).

We further probed the mechanism underlying the cellular internalization of zwitterionic polymers based lipoplexes by performing the cellular uptake study at 4 °C or in the presence of various endocytic inhibitors. As shown in Fig. 6, the cell internalization of these three lipoplexes was energy-dependent process as about 65.0% of the cellular uptake was blocked at 4 °C mβCD, chlorpromazine and dynasore all significantly inhibited the cellular uptake level of both zwitterionic polymer modified lipoplexes, indicating that the lipoplexes were also internalized *via* both the caveolae- and clathrin-mediated endocytosis pathways [38].

3.7. Endosomal/lysosomal escape of the lipoplexes

Cationic liposomes entered cells *via* both the caveolae- and clathrin-mediated endocytosis, which led to the delivery of the lipoplexes to endosomes/lysosomes. Therefore, the lipoplexes needed to escape from the endosomes/lysosomes as the siRNA produced its effects in the cytoplasm. Thus, the endosomal/lysosomal escape of the lipoplexes was evaluated in Hela cells after 2 h and 4 h incubation, respectively. As shown in Fig. 7A, there were a relatively high co-localization spots of the green FAM-siRNA and red endosomes/lysosomes for 2 h, indicating that the major of the three lipoplexes were within endosomes/lysosomes. The green FAM-siRNA fluorescence was almost total separated from the endosomes/lysosomes after 4 h incubation for CPT-PCB_6 and DSPE-PCB_6 CPT lipoplexes, indicating the successful endosomal/lysosomal escape. However, the green FAM-siRNA fluorescence of CPT-$PMPC_6$ lipoplexes still partially colocalized with the red fluorescence, suggesting that siRNA was still within endosomes/lysosomes. The quantitative result of co-localization ratio for CPT-PCB_6 lipoplexes decreased about 49%, while only 19% for CPT-$PMPC_6$ lipoplexes (Fig. 7B). The results indicated that the pH-sensitive PCB modified lipoplexes had higher endosomal/lysosomal escape ability than that of PMPC modified lipoplexes due to the protonation of PCB in acidic environment, which could accelerated the endosomal/lysosomal escape of siRNA.

The localization of CPT in cells was additionally observed by CLSM after 4 h and 12 h of incubation, respectively. As shown in Fig. 8, the separation of CPT and FAM-siRNA at 4 h for CPT-PCB_6 and DSPE-PCB_6 CPT lipoplexes indicated the successful endosomal/lysosomal escape of the siRNA into cytoplasm. Compared with DSPE-PCB_6 CPT lipoplexes, most of the CPT for CPT-PCB_6 lipoplexes remained in the cytoplasm after 4 h of incubation due to its sustained release behavior and the CPT entered nucleus after 12 h of incubation. The results confirmed that the CPT-PCB_6 lipoplexes released siRNA and CPT in a temporally controlled release manner. First, the CPT-PCB_6 lipoplexes accelerated the endosomal/lysosomal escape of siRNA after 4 h incubation due to the protonation of PCB. Second, CPT was released in a sustained manner in response to pH and esterase and then highly accumulated in nucleus after 12 h of incubation. However, the delayed endosomal/lysosomal escape of CPT-$PMPC_6$ lipoplexes impeded its release of siRNA into cytoplasm and CPT into nucleus.

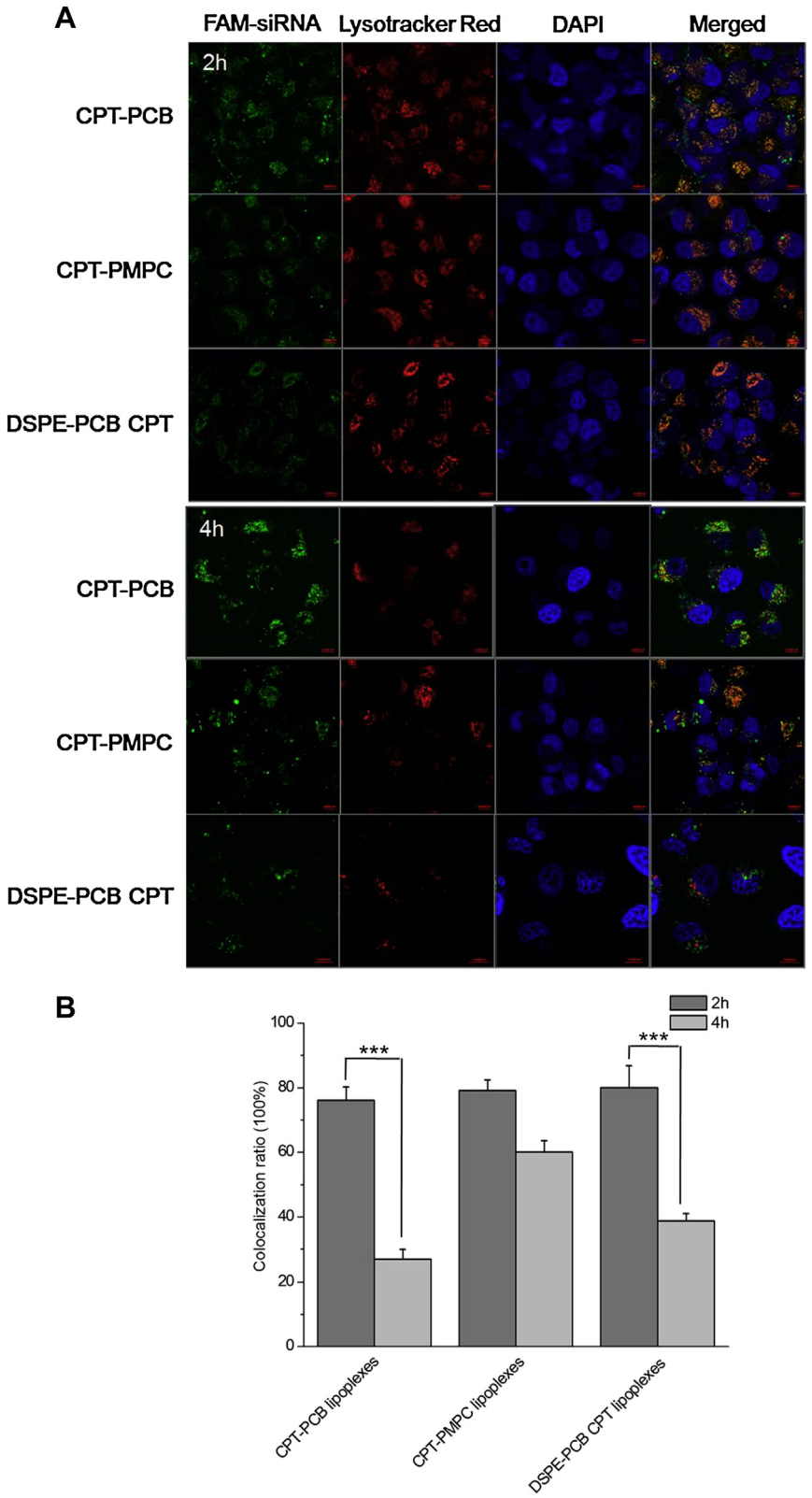

Fig. 7. (A) Assessment by confocal laser scanning microscopy (CLSM) of endosomal/lysosomal escape of CPT-PCB_6, CPT-$PMPC_6$ and DSPE-PCB_6 CPT lipoplexes with FAM-siRNA in Hela cells after 2 h and 4 h of incubation. The endosomes/lysosomes and cell nucleus were counterstained with Lysotracker Red and DAPI, respectively. (Scale bar: 10 μm). (B) The co-localization ratio of fluorescence intensity of FAM-siRNA and Lysotracker Red was qualified with CLSM. The concentration of FAM-siRNA was 1 μg/mL for each well. $^{*}P < 0.05$, $^{**}P < 0.01$, $^{***}P < 0.005$ ($n = 3$). (For interpretation of the references to colour in this figure legend, the reader is referred to the web version of this article.)

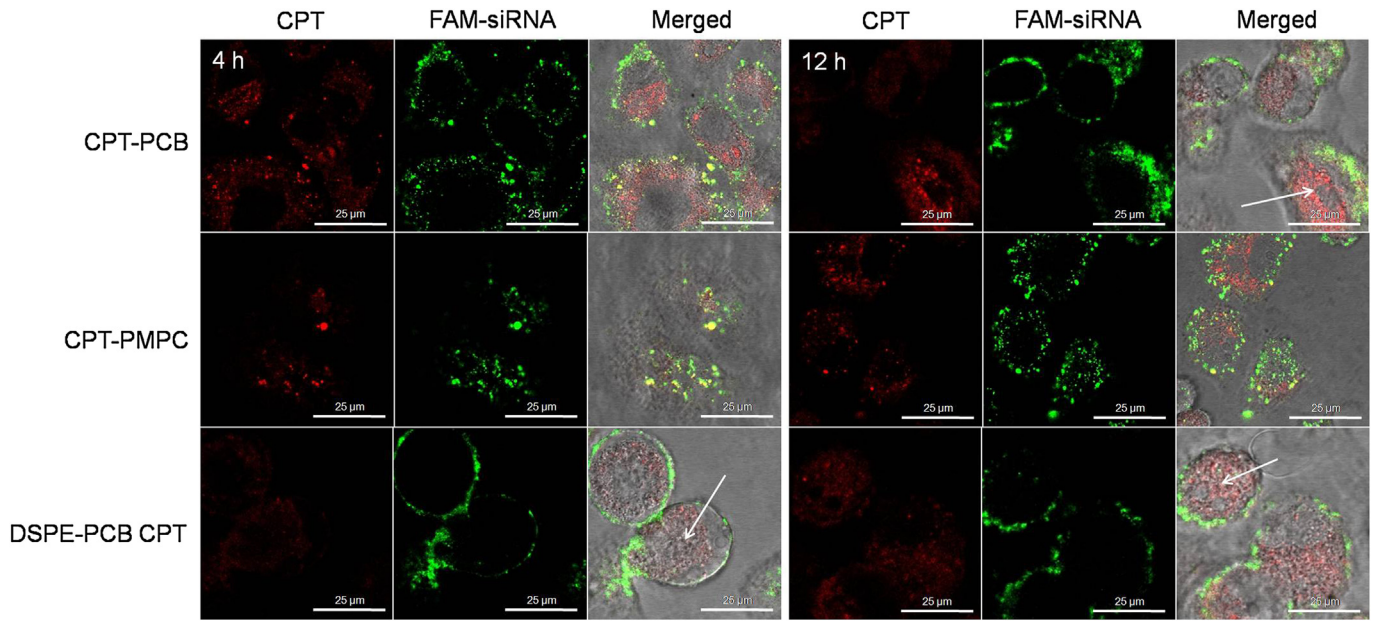

Fig. 8. Confocal laser scanning microscopy (CLSM) images of the intracellular distribution of CPT-PCB_6, CPT-$PMPC_6$ and DSPE-PCB_6 CPT lipoplexes with FAM-siRNA in Hela cells after 4 h and 12 h of incubation at 37 °C, respectively. (Scale bar: 25 μm).

3.8. *In vitro gene silencing efficiency of the lipoplexes*

Excellent endosomal/lysosomal escape ability could promote the gene silencing efficiency of the non-viral gene vector. The gene silencing efficiency of the dual sensitive CPT-PCB_6 lipoplexes was evaluated in Hela cells. Polo-like kinase 1 (Plk1) was selected as the oncogenic target since it is a well known key regulator of the mitotic progression of mammalian cells and its activity is elevated in many cancer cells [39]. It has been proved that the treatment of tumor cells with siRNA targeting Plk1 could improve the sensitivity of cancer cells to CPT and CPT exerts more cytotoxicity. The level of Plk1 mRNA in Hela cells after 24 h incubation was analyzed by qRT-PCR. As shown in Fig. 9A, the down-regulation efficiency for naked siPlk1 was only 27.0% due to its lower level of cellular uptake. In contrast, the down-regulation efficiency for CPT-PCB_6 cationic liposomes with siPlk1 was 81.9%, which was much larger than that of

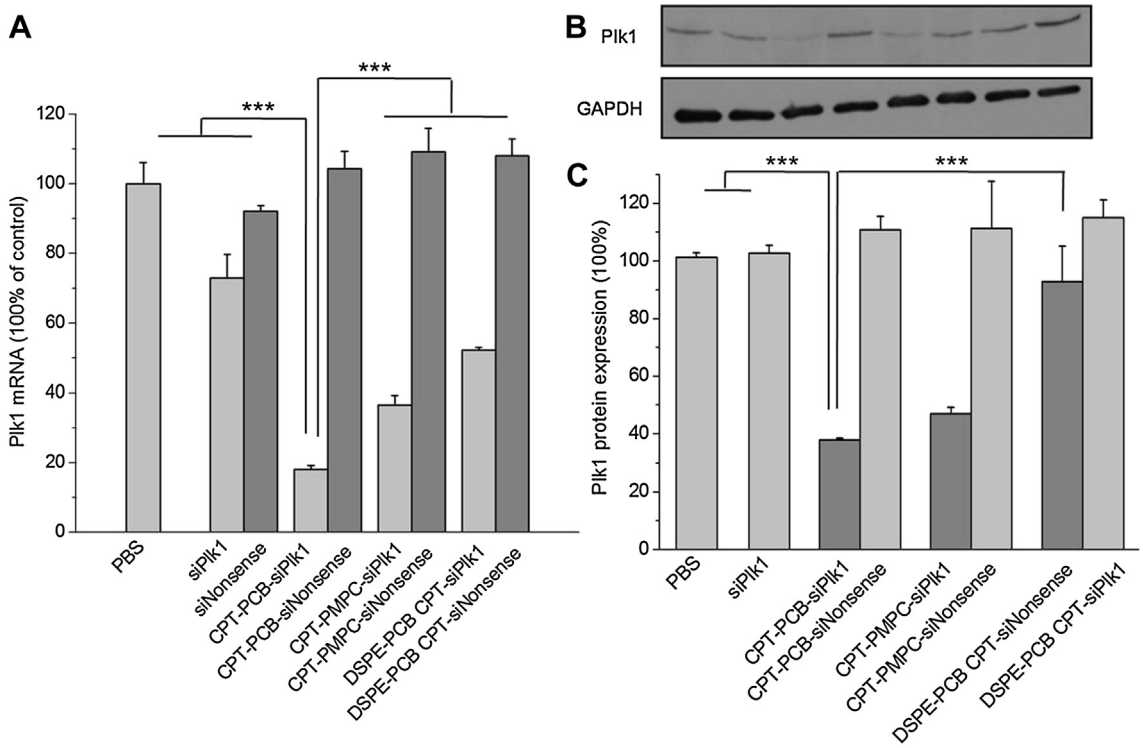

Fig. 9. (A) Expression of Plk1 mRNA determined by qRT-PCR. (B) Representative Plk1 protein expression determined by WB analysis. (C) Analysis of light intensities of Plk1 protein expression as the ratio of Plk1 to GAPDH from WB results. Transfection experiments were performed independently three times. $^{*}P < 0.05$, $^{**}P < 0.01$, $^{***}P < 0.005$ ($n = 3$).

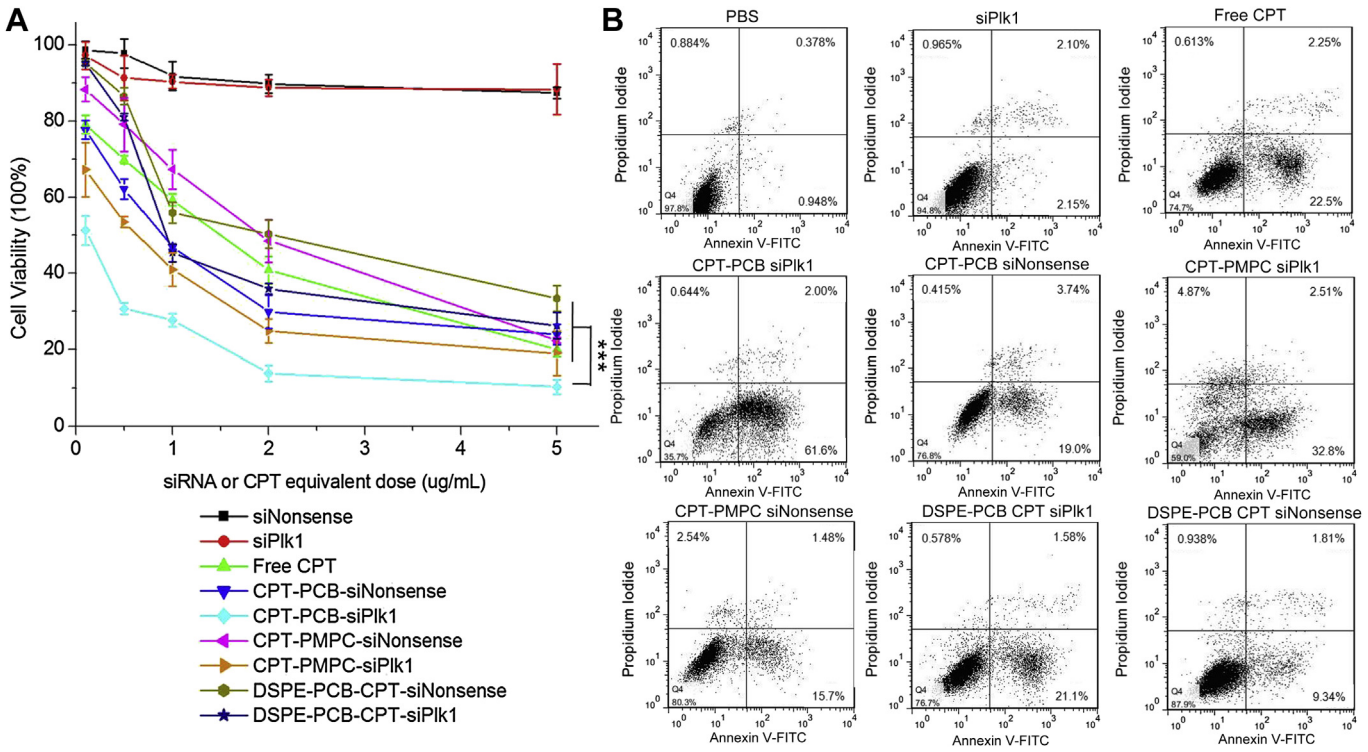

Fig. 10. (A) *In vitro* cytotoxicity of CPT-based lipoplexes with various concentration of siRNA on Hela cells after 72 h of incubation. The concentration of free CPT was equal to the concentration of CPT for CPT-PCB_6 lipoplexes corresponding to each siRNA concentration. The cell viability was detected using MTT assay. (B) Induction of apoptosis on Hela cells by naked siRNA, free CPT and lipoplexes formulation. The early apoptosis cells are presented in the lower right quadrant, and fully apoptosis cells are presented in the upper right quadrant. Data are shown as the mean ± S.D. of three independent experiments. $^{*}P < 0.05$, $^{**}P < 0.01$, $^{***}P < 0.005$ ($n = 3$).

CPT-$PMPC_6$ (63.4%) and DSPE-PCB_6 CPT (47.9%) lipoplexes. It was worth noting that cationic liposomes carrying negative control siRNA did not show a significant gene silencing effect, implying that no nonspecific gene silencing occurred. To examine whether the reduction in Plk1 mRNA was subsequently accompanied by the decreased Plk1 expression, the Plk1 protein expression was detected by WB analyses. As shown in Fig. 9B and C, free siPlk1 did not show any efficiency in the down-regulation of Plk1 protein expression in Hela cells. The Plk1 protein expression was about 46.9% and 92.8% for CPT-$PMPC_6$ and DSPE-PCB_6 CPT lipoplexes, respectively, whereas the CPT-PCB_6 lipoplexes would significantly knockdown Plk1 protein expression to a lower level of 37.7%. The results demonstrated that the dual sensitive CPT-PCB lipoplexes with superior cellular uptake and endosomal/lysosomal escape ability could significantly improve targeting gene silencing efficiency.

3.9. *In vitro antitumor activity of the lipoplexes*

It has been proved that the treatment of Hela cells with siRNA targeting Plk1 could improve the sensitivity of cancer cells to CPT. Synergistically inhibition effect on Hela cells of the CPT-PCB_6 siPlk1 lipoplexes was detected using MTT assay (Fig. 10A). As indicated, simultaneous delivery of siPlk1 with CPT-PCB_6 prodrug system significantly reduced cell viability to approximately 13.9% at siPlk1 concentration of 3 μg/mL, while the cell viability was 30.0% for CPT-PCB_6/siNonsense lipoplexes. The cytotoxicity of CPT-PCB_6 lipoplexes was much higher than other formulations at the same concentration of siRNA due to its temporally controlled release behavior and excellent siPlk1 gene silencing efficiency.

Knockdown of Plk1 has been shown to induce apoptosis in tumor cells. Apoptosis was evaluated after treating Hela cells with formulations containing 2 μg siRNA/mL, and then stained with Annexin V-FITC Apoptosis Detection Kit I (Fig. 10B). CPT-PCB_6/siNonsense lipoplexes induced cell apoptosis to 22.7%, but not surprisingly, simultaneous delivery of siPlk1 with the CPT-PCB_6 system could increase cell apoptosis to 63.6%, with a synergistic effect as well, which was clearly higher than that of other combinatorial delivery system (CPT-$PMPC_6$/siPlk1 lipoplexes 41.0%, DSPE-PCB_6 CPT/siPlk1 lipoplexes 23.3%).

3.10. *Pharmacokinetics profiles and biodistribution of the lipoplexes*

The developed dual sensitive CPT-PCB/siPlk1 lipoplexes have been shown excellent antitumor activity *in vitro*. In order to evaluate the potential of antitumor activity of the dual sensitive CPT-PCB_6/siPlk lipoplexes *in vivo*, the biodistribution of the lipoplexes after 24 h of intravenous injection in Hela-bearing nude mice was evaluated. As shown in Fig. 11A–C, all of the lipoplexes enhanced the siRNA accumulation in tumor compared with naked siRNA. With the same siRNA injected dose, the fluorescence intensity of Cy5-siRNA for CPT-PCB_6 lipoplexes was higher than that of DSPE-PCB_6 CPT lipoplexes due to their excellent serum stability. At the same time, the tumor accumulation of CPT for CPT-PCB_6 lipoplexes was stronger than that of CPT-$PMPC_6$ and DSPE-PCB_6 CPT lipoplexes due to their higher CPT loading content (Fig. 11D). As shown in Fig. 11E, with the same CPT injected dose, the concentration of CPT in plasma for CPT-PCB_6 and CPT-$PMPC_6$ lipoplexes was comparable, which was about 2 times of that for DSPE-PCB_6 CPT lipoplexes. This was probably because easily burst release behavior of DSPE-PCB_6 CPT lipoplexes reduced the circulation time of CPT.

3.11. *In vivo antitumor activity of the lipoplexes*

The dual sensitive CPT-PCB_6/siPlk1 lipoplexes potentially enhanced the antitumor activity in synergistically manner *in vitro*

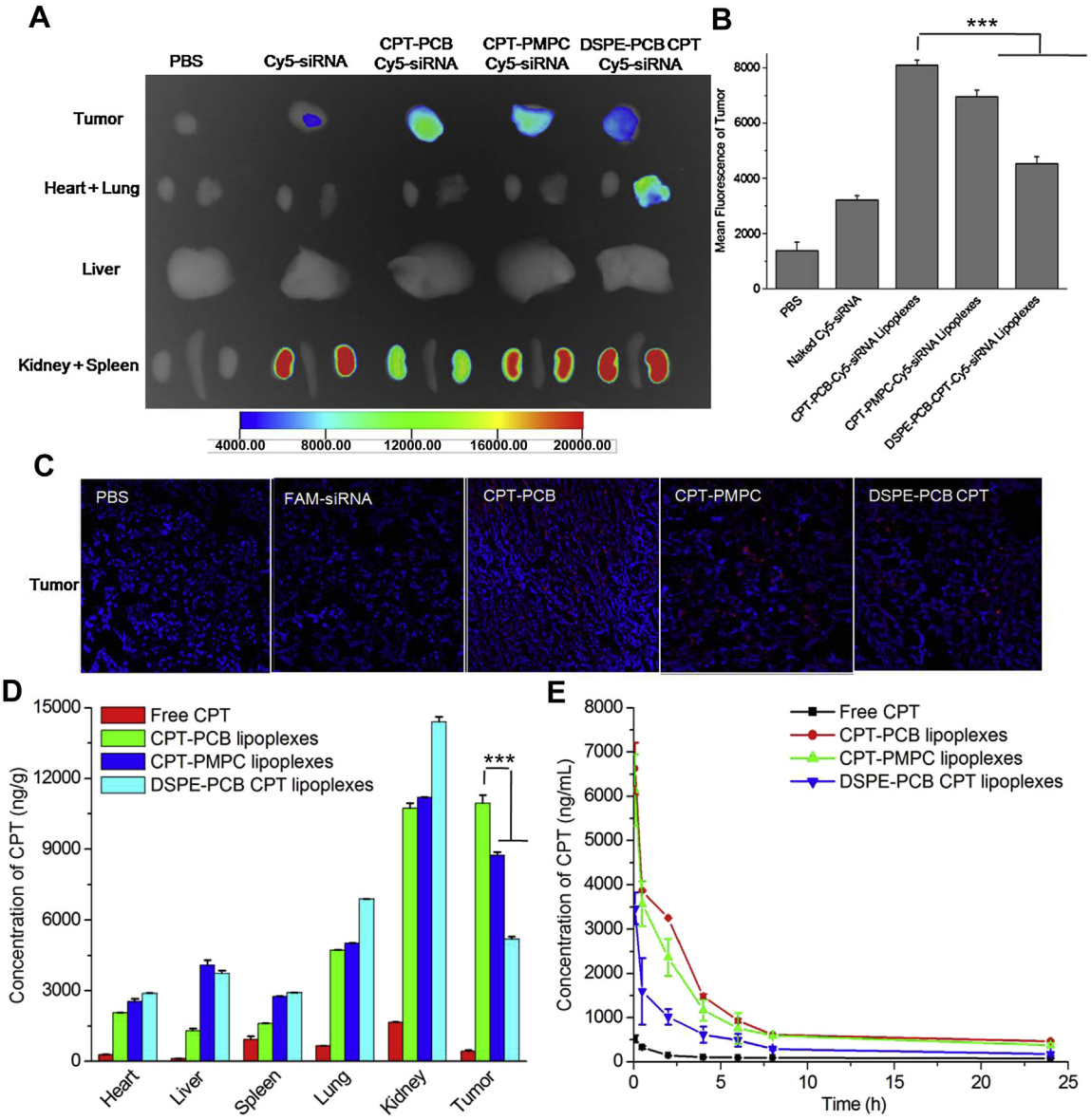

Fig. 11. *In vivo* distribution after intravenous injection of free Cy5-siRNA, free CPT and CPT-based lipoplexes to Hela tumor-bearing nude mice. (A) Cy5 fluorescent images of tissues distribution. (B) The fluorescence intensity of Cy5-siRNA in tumor tissue examined with a Kodak *in vivo* imaging system. (C) CLSM images show the distribution of Cy5-siRNA in tumor. (D) The biodistribution of CPT in organs. Lipoplexes with Cy5-siRNA were administered to each mouse *via* tail vein injection at 2.0 mg Cy5-siRNA/kg. (E) The concentration of CPT in plasma as a function of time post-injection. Lipoplexes were administered to each ICR mouse *via* tail vein injection at 4.0 mg CPT/kg. Data are shown as the mean ± S.D. of three independent experiments. $^{*}P < 0.05$, $^{**}P < 0.01$, $^{***}P < 0.005$ ($n = 3$).

and had strong tumor accumulation *in vivo*. To detect the antitumor activity of lipoplexes *in vivo*, the antitumor growth effect in Hela tumor-bearing nude mice was performed of different formulations carrying siPlk1 *via* tail vein injection. As illustrated in Fig. 12A, treatment with the siPlk1 and CPT alone did not show significantly tumor growth inhibition in comparison with PBS groups. CPT-PCB_6/siNonsense lipoplexes slightly inhibited tumor growth with the final relative tumor volume (RTV) of 264.6%. In comparison, formulations codelivery of CPT and siPlk1 showed a significant inhibition efficiency of tumor growth especially the CPT-PCB_6/siPlk1 lipoplexes with the RTV of 114.5% due to its excellent tumor accumulation and synergistic manner, which was also much higher than that of CPT-$PMPC_6$/siPlk1 lipoplexes (210.6%) and DSPE-PCB_6 CPT/siPlk1 lipoplexes (256.2%). Compared with free CPT, the CPT-based lipoplexes exhibited neglectable toxicity, which indicated the good biocompability of PCB and PMPC modified lipoplexes (Fig. 12B).

To further evaluate whether retarded tumor growth by codelivery system was related to Plk1 gene silencing in tumor cells, the tumor mass was excised 24 h after the last injection. Mice treated with CPT-PCB_6/siPlk1 lipoplexes showed reduced Plk1 mRNA levels to about 40.5% of the PBS control, whereas other formulations exhibited only slight down-regulation of Plk1 mRNA, about 19.4% for CPT-$PMPC_6$ lipoplexes and 23.3% for DSPE-PCB_6 CPT lipoplexes (Fig. 12C). As shown in Fig. 12D, analysis of Plk1 protein of each tumor mass by WB analyses showed the consistent knockdown efficiency. Cell apoptosis in tumors treated with various formulations was analyzed by TUNEL (Fig. 12E), that the CPT-PCB_6 lipoplexes with siPlk1 induced more significant cell apoptosis in tumors. The results demonstrated that the dual sensitive CPT-PCB_6/siPlk1 lipoplexes with higher tumor accumulation of payloads and synergistically inhibition effect exhibited excellent antitumor activity in a combination manner.

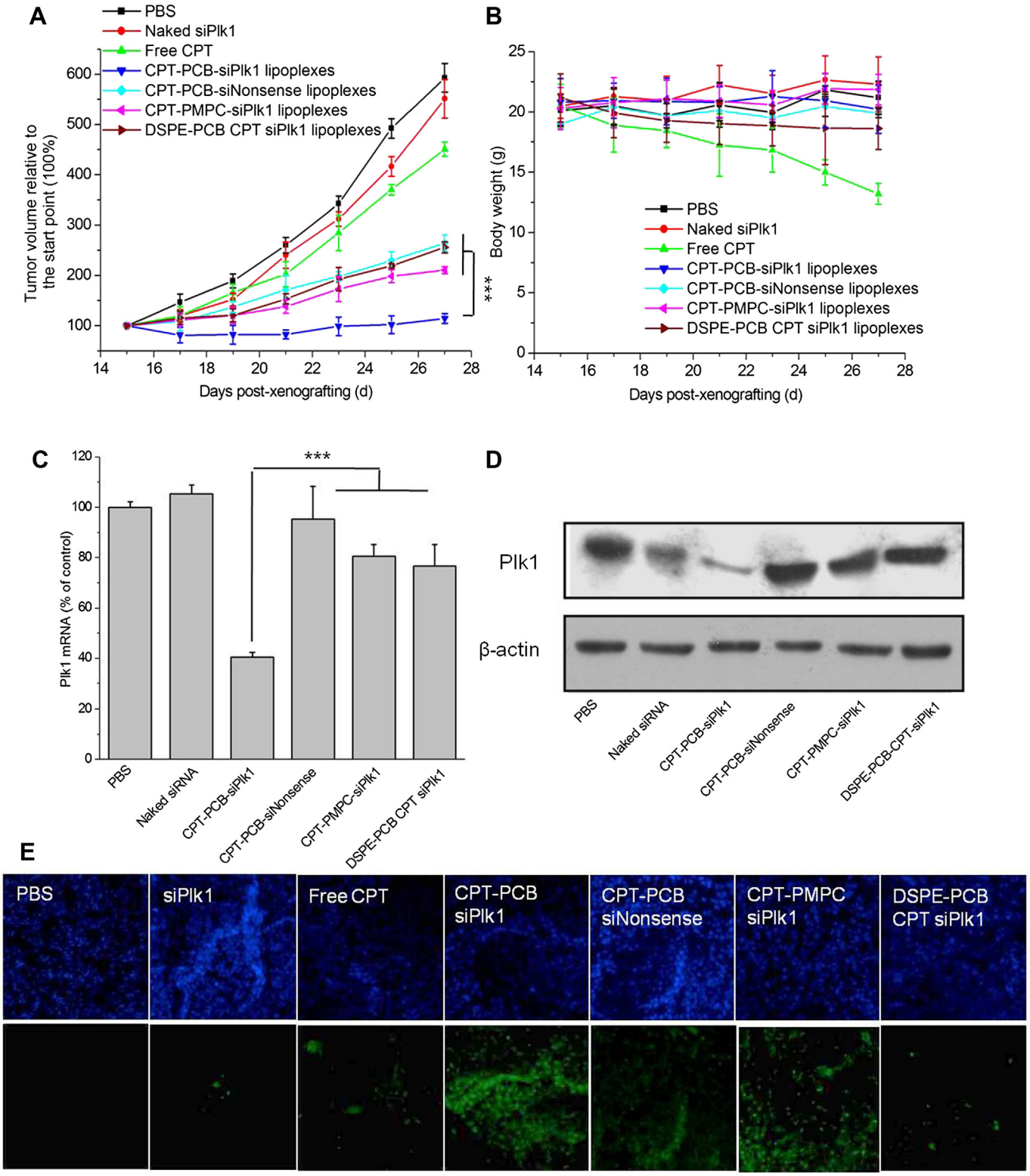

Fig. 12. (A) Inhibition of Hela tumor growth by CPT-PCB/siPlk1 lipoplexes in comparison with other formulations. (B) The body weight changes. (C) Expression of Plk1 mRNA in tumor determined by qRT-PCR. (D) Representative Plk1 protein expression in tumor determined by WB analysis. (E) TUNEL analyses of tumor tissue. Hela tumor-bearing nude mice received one injection with 2.5 mg siRNA/kg *via* the tail vein injection every other day. The tumor tissue were collected after 12 days of treatment ($n = 5$). $^{*}P < 0.05$, $^{**}P < 0.01$, $^{***}P < 0.005$.

4. Conclusion

In summary, we successfully developed dual sensitive and temporally controlled CPT prodrug based cationic liposomes for siPlk1 codelivery for cancer therapy. Quite different from the DSPE-PCB CPT non-covalent encapsulated lipoplexes and non pH-sensitive PMPC modified CPT-PMPC prodrug lipoplexes, the dual sensitive CPT-PCB/siPlk1 lipoplexes with higher CPT loading content could enhance the serum stability of lipoplexes and achieve temporally controlled release of siRNA and CPT due to the

protonation of PCB in endosomes/lysosomes and the pH and esterase-sensitive of CPT-PCB prodrug. As a result, the dual sensitive codelivery system had excellent antitumor activity *in vitro* and *in vivo* in a synergistic manner, which provided a promising approach for effective combination therapy.

Acknowledgment

This work was financially supported by the National Natural Science Foundation of China (21304099, 51203162, 51103159, 51373177), the National High Technology Research and Development Program (2014AA020708, 2012AA022703, 2012AA020804), the Instrument Developing Project of the Chinese Academy of Sciences (YZ201253, YZ201313), the Open Funding Project of the National Key Laboratory of Biochemical Engineering (Y22504A169) and the "Strategic Priority Research Program" of the Chinese Academy of Sciences (XDA09030301-3).

Appendix A. Supplementary data

Supplementary data related to this article can be found at http://dx.doi.org/10.1016/j.biomaterials.2014.08.022.

References

[1] Dong DW, Xiang B, Gao W, Yang ZZ, Li JQ, Qi XR. pH-responsive complexes using prefunctionalized polymers for synchronous delivery of doxorubicin and siRNA to cancer cells. Biomaterials 2013;34:4849–59.
[2] Sun TM, Du JZ, Yao YD, Mao CQ, Dou S, Huang SY. Simultaneous delivery of siRNA and paclitaxel *via* a "two-in-one" micelleplex promotes synergistic tumor suppression. ACS Nano 2011;5:1483–94.
[3] Yu BJ, Tang C, Yin CH. Enhanced antitumor efficacy of folate modified amphiphilic nanoparticles through co-delivery of chemotherapeutic drugs and genes. Biomaterials 2014;35:6369–78.
[4] Liu HM, Li Y, Mozhi A, Zhang L, Liu YL, Xu X. SiRNA-phospholipid conjugates for gene and drug delivery in cancer treatment. Biomaterials 2014;35:6519–33.
[5] Ci TY, Li T, Chang GT, Yu L, Ding JD. Simply mixing with poly(ethylene glycol) enhances the fraction of the active chemical form of antitumor drugs of camptothecin family. J Control Release 2013;169:329–35.
[6] Li XQ, Wen HY, Dong HQ, Xue WM, Pauletti GM, Cai XJ, et al. Self-assembling nanomicelles of a novel camptothecin prodrug engineered with a redox-responsive release mechanism. Chem Commun 2011;47:8647–9.
[7] Liu J, Jiang ZZ, Zhang SM, Saltzman WM. Poly(ω-pentadecalactone-*co*-butylene-*co*-succinate) nanoparticles as biodegradable carriers for camptothecin delivery. Biomaterials 2009;30:5707–19.
[8] Fan P, Zhang S, Tian H, Yan N, Dai L, Zhang X, et al. Enhanced chemosensitivity to CPT-11 in colorectal xenografts by small hairpin RNA interference targeting PLK1. Neoplasma 2012;59:676–84.
[9] Kreis NN, Sommer K, Sanhaji M, Kramer A, Matthess Y, Kaufmann M, et al. Long-term downregulation of Polo-like kinase 1 increase the cyclin-dependent kinase inhibitor p21 WAF1/CIP1. Cell Cycle 2009;8:460–72.
[10] Mao CQ, Du JZ, Sun TM, Yao YD, Zhang PZ, Song E, et al. A biodegradable amphiphilic and cationic triblock copolymer for the delivery of siRNA targeting the acid ceramidase gene for cancer therapy. Biomaterials 2011;32:3124–33.
[11] Hu XL, Tian J, Liu T, Zhang GY, Liu SY. Photo-triggered release of caged camptothecin prodrugs from dually responsive shell cross-linked micelles. Macromolecules 2013;46:6243–56.
[12] Yurkovetskiy AV, Hiller A, Syed S, Yin M, Lu XM, Fischman AJ, et al. Synthesis of a macromolecular camptothecin conjugate with dual phase drug release. Mol Pharm 2004;1:375–82.
[13] Liu XL, Lynn BC, Zhang JH, Song L, Bom D, Du W, et al. A versatile prodrug approach for liposomal core-loading of water-insoluble camptothecin anticancer drugs. J Am Chem Soc 2002;124:7650–1.
[14] Saad M, Garbuzenko OB, Minko T. Co-delivery of siRNA and an anticancer drug for treatment of multidrug-resistant cancer. Nanomedicine 2008;3:761–76.
[15] Wei W, Lv PP, Chen XM, Yue ZG, Fu Q, Liu SY, et al. Codelivery of mTERT siRNA and paclitaxel by chitosan-based nanoparticles promoted synergistic tumor suppression. Biomaterials 2013;34:3912–23.
[16] Duan XP, Xiao JS, Yin Q, Zhang ZW, Yu HJ, Mao SR, et al. Smart pH-sensitive and temporal-controlled polymeric micelles for effective combination therapy of doxorubicin and disulfiram. ACS Nano 2013;7:5858–69.
[17] Greco F, Vicent MJ. Combination therapy: opportunities and challenges for polymer-drug conjugates as anticancer nanomedicines. Adv Drug Deliv Rev 2009;61:1203–13.
[18] Zhou ZX, Shen YQ, Tang JB, Fan MH, Kirk EAV, Murdoch WJ, et al. Charge-reversal drug conjugate for targeted cancer cell nuclear drug delivery. Adv Funct Mater 2009;19:3580–9.
[19] Tong R, Cheng JJ. Paclitaxel-initiated, controlled polymerization of lactide for the formulation of polymeric nanoparticulate delivery vehicles. Angew Chem Int Ed 2008;47:4830–4.
[20] Shen YQ, Jin E, Zhang B, Murphy CJ, Sui MH, Zhao J, et al. Prodrugs forming high drug loading multifunctional nanocapsules for intracellular cancer drug delivery. J Am Chem Soc 2010;132:4259–65.
[21] Lee ES, Na K, Bae YH. Doxorubicin loaded pH-sensitive polymeric micelles for reversal of resistant MCF-7 tumor. J Control Release 2005;103:405–18.
[22] Wu Q, Du F, Luo Y, Lu W, Huang J, Yu JH, et al. Poly(ethylene glycol) shell-sheddable nanomicelle prodrug of camptothecin with enhanced cellular uptake. Colloid Surfaces B 2013;105:294–302.
[23] Paranjpe PV, Chen Y, Kholodovych V, Welsh W, Stein S, Sinko PJ. Tumor-targeted bioconjugate based delivery of camptothecin: design, synthesis and *in vitro* evaluation. J Control Release 2004;100:275–92.
[24] Chan CL, Majzoub RN, Shirazi RS, Ewert KK, Chen YJ, Liang KS, et al. Endosomal escape and transfection efficiency of PEGylated cationic liposome-DNA complexes prepared with an acid-labile PEG-lipid. Biomaterials 2012;33:4928–35.
[25] Hatakeyama H, Akita H, Kogure K, Oishi M, Nagasaki Y, Kihira Y, et al. Development of a novel systemic gene delivery system for cancer therapy with a tumor-specific cleavable PEG-lipid. Gene Ther 2007;14:68–77.
[26] Hatakeyama H, Ito E, Akita H, Oishi M, Nagasaki Y, Futaki S, et al. A pH-sensitive fusogenic peptide facilitates endosomal escape and greatly enhances the gene silencing of siRNA-containing nanoparticles *in vitro* and *in vivo*. J Control Release 2009;139:127–32.
[27] Wang JQ, Sun XR, Mao WW, Sun WL, Tang JB, Sui MH, et al. Tumor redox heterogeneity-responsive prodrug nanocapsules for cancer chemotherapy. Adv Mater 2013;25:3670–6.
[28] Greenwald RB, Choe YH, McGuire J, Donover CD. Effective drug delivery by PEGylated drug conjugates. Adv Drug Deliv Rev 2003;55:217–50.
[29] Tang Q, Cao B, Cheng G. Co-delivery of small interfering RNA using a camptothecin prodrug as the carrier. Chem Commun 2014;50:1323–5.
[30] Li Y, Cheng Q, Jiang Q, Huang YY, Liu HM, Zhao YL, et al. Enhanced endosomal/lysosomal escape by distearoyl phosphoethanolamine-polycarboxybetaine lipid for systemic delivery of siRNA. J Control Release 2014;176:104–14.
[31] Chen XJ, McRae S, Parelkar S, Emrick T. Polymeric phosphorylcholine-camptothecin conjugates prepared by controlled free radical polymerization and click chemistry. Bioconjug Chem 2009;20:2331–41.
[32] Kataoka K, Harada A, Nagasaki Y. Block copolymer micelles for drug delivery: design, characterization and biological significance. Adv Drug Deliv Rev 2001;47:113–31.
[33] Maeda H, Wu J, Sawa T, Matsumura Y, Hori K. Tumor vascular permeability and the EPR effect in macromolecular therapeutics: a review. J Control Release 2000;65:271–84.
[34] Talukdar Y, Rashkow JT, Lalwani G, Kanakia S, Sitharaman B. The effects of graphene nanostructures on mesenchymal stem cells. Biomaterials 2014;35:4863–77.
[35] Ke CJ, Su TY, Chen HL, Liu HL, Chiang WL, Chu PC, et al. Smart multifunctional hollow microspheres for the quick release of drugs in intracellular lysosomal compartments. Angew Chem Int Ed 2011;123:8236–9.
[36] Funhoff AM, Nostrum CFV, Koning GA, Schuurmanns-Nieuwenbroek NME, Crommelin DJA, Hennink WE. Endosomal escape of polymeric gene delivery complexes is not always enhanced by polymers buffering at low pH. Biomacromolecules 2004;5:32–9.
[37] Li XJ, Takashima M, Yuba E, Harada A, Kono K. PEGylated PAMAM dendrimer-doxorubicin conjugat-hybridized gold nanorod for combined photothermal-chemotherapy. Biomaterials 2014;35:6576–84.
[38] Yin LC, Song ZY, Kim KH, Zheng N, Tang HY, Lu H. Reconfiguring the architectures of cationic helical polypeptides to control non-viral gene delivery. Biomaterials 2013;34:2340–9.
[39] Yang XZ, Dou S, Sun TM, Mao CQ, Wang HX, Wang J. Systemic delivery of siRNA with cationic lipid assisted PEG-PLA nanoparticles for cancer therapy. J Control Release 2011;156:203–11.